(Received 25 July 2024, Accepted 11 October 2024, Scheduled 21 October 2024)

Double Closed-Loop Model-Free Super-Twisting Terminal Sliding Mode Control Algorithm of IPMSM Based on Third-Order Super-Twisting Observer

Qianghui Xiao[1], Zhi Wang[1], Xiaorui Wei[1], Yuxin Yang[1], Yushuang Zhang[1], and Zhun Cheng[2,*]

[1]*Hunan University of Technology, Zhuzhou 412007, China*
[2]*Hunan Railway Professional Technology College, Zhuzhou 412001, China*

ABSTRACT: To solve the problem of poor control performance of internal permanent magnet synchronous motors (IPMSM) due to parameter perturbations and external perturbations when adopting mode-free sliding mode control (MFSMC) algorithm, a double-closed-loop model-free super-twisting terminal sliding mode control (MFSTTSMC) algorithm of IPMSM based on third-order super-twisting observer (TOSTO) is proposed. Firstly, according to the new model-free control (MFC) algorithm, an ultra-local expansion model of IPMSM speed-current double closed-loop is established. Secondly, based on the ultra-local expansion model, a double closed-loop MFSTTSMC is designed to achieve global rapid convergence of system state errors. At the same time, a TOSTO is designed to estimate the disturbance in real time and carry out feedforward compensation, which enhances system robustness. Finally, the viability and superiority of the proposed control algorithm is demonstrated through simulation and experiments.

1. INTRODUCTION

In recent years, internal permanent magnet synchronous motors (IPMSMs) have been widely used in traction systems, servo drive systems, and household appliances due to their good performance [1, 2]. However, IPMSM is a nonlinear multivariable coupling system, and when the motor is running under complex working conditions, the parameters such as flux and *d*-*q* axis inductance of the motor fluctuate with the change of temperature and working conditions [3]. These changes can bring uncertain disturbance variables to the controller, which will affect the overall control performance of the motor, resulting in unsatisfactory control results in high-performance applications. Therefore, it is of great significance to adopt better control algorithms to ensure the stable operation of the motor under complex working conditions [4].

With the deepening of theoretical research, many excellent control algorithms have been applied to the drive system of PMSM, such as adaptive control [5, 6], modulo predictive control [7, 8], robust control [9, 10], sliding mode control (SMC) [11–13], and model-free control (MFC) [14–16]. Among them, MFC was proposed by Fliess and Join, which has excellent robustness to systems with unknown parameters and complex coupling structures [14]. Ref. [15] analyzes the ultra-local model in MFC and proposes an adaptive model-free control, which uses the adaptive law to perform online parameter tuning, reducing the workload of related parameter tuning. In [16], a model-free control method was applied to the SPMSM speed control system, and the influence of parameter changes was eliminated by designing a model-free current controller.

At the same time, SMC has the advantages of simple algorithm and strong robustness to external interference [17]. With the deepening of the research of MFC algorithms in the field of motor control, relevant scholars have combined MFC and SMC to realize the composite control algorithm of Model-Free Sliding Mode Control (MFSMC). In [18], an MFC method based on sliding mode was proposed, which used a sliding mode observer to estimate the uncertainty in the ultra-local model, and the experimental results proved the feasibility of the composite control method. However, the traditional sliding surface is in an asymptotic convergence state, and the convergence speed is slow. Compared to the conventional sliding form, the terminal sliding mode of the high-order sliding surface can achieve finite time convergence, but there are singular problems [19]. In [20], a fast non-singular terminal sliding Mode (FNTSM) was designed to effectively solve the singular problem in the terminal sliding mode. In [21], an MFFNTSMC algorithm was designed based on the MFC algorithm to effectively speed up the response of the motor, but the influence of the motor on the system under the failure of magnetism loss was not considered. In [22], a model-free predictive control algorithm has been proposed to enable the motor to suppress system disturbances during demagnetisation faults, and the algorithm achieves good control results, but the system tracking error needs to be increased.

In the design of an MFSMC controller, the above methods ignore the observation accuracy of the uncertain variables in the ultra-local model, and directly use the traditional sliding mode observer to estimate the uncertain variables, resulting in low observation accuracy and reducing the control effect of the motor.

* Corresponding author: Zhun Cheng (120277982@qq.com).

In [23], the ultra-local model was extended, and an extended sliding mode observer (ESMO) was designed to effectively improve the observation accuracy. In [24], a position-free control method for ESMO was proposed, which was used to estimate the position of the rotor, and the feasibility and effectiveness of the method in the case of drive system failure were verified by experiments, but ESMO was designed for first-order sliding mode, and the observer still had large jitter. In [25], a super-twisting observer (STO) is proposed, and the super-twisting algorithm of the high-order sliding mode can effectively weaken the jitter phenomenon on the low-order sliding mode, and the experimental results show that the observation accuracy of the super-twisting observer is better, but the convergence speed of the super-twisting algorithm is affected by the integral term, and the dynamic performance of the observer is poor. Therefore, it is of great significance to design a model-free sliding mode control method with accurate dynamic observation and strong transient performance.

To solve the problem of poor control performance of IPMSM due to parameter perturbations and external perturbations when adopting MFSMC algorithm, a double-closed-loop model-free super-twisting terminal sliding mode control (MFSTTSMC) algorithm of IPMSM based on the third-order super-twisting observer (TOSTO) is proposed. Firstly, according to the mathematical model of IPMSM speed-current loop, a double-closed-loop ultra-local expansion model is established. Secondly, a super-twisting non-singular integral terminal sliding mode is designed to make the systematic error converge quickly and stably in the global world, and a double closed-loop MFSTTSMC based on speed-current loop is designed by combining the new MFC algorithm. For the nonlinear perturbation variables in the ultra-local expansion model, a TOSTO algorithm is designed to estimate the perturbation variables and realize feedforward compensation. Finally, the feasibility and effectiveness of the proposed control method are verified by comparing the simulation and semi-physical experiments of MFSMC and STO-MFSMC.

2. ULTRA-LOCAL EXPANSION MODEL OF IPMSM

Considering the influence of parameters, a mathematical model of IPMSM in the d-q axis coordinate system is established:

$$\begin{cases} u_d = R_s i_d + L_d \dot{i}_d - \omega_e L_d i_q + \Delta u_d \\ u_q = R_s i_q + L_q \dot{i}_q + \omega_e (L_q i_d + \psi_m) + \Delta u_q \\ \dot{\omega}_e = p_n (T_e - B\omega_m - T_L + \Delta T_e)/J \end{cases} \tag{1}$$

where u_d and u_q represent the stator voltage components under the decoupling of the d-q axis coordinate system, respectively; i_d and i_q represent the d-axis current and q-axis current, respectively; L_d and L_q represent the d-axis inductance and q-axis inductance, respectively; R_s is the stator resistance; ψ_m is the flux of a permanent magnet; p_n represents the number of pole pairs of the motor; ω_e represents the angular velocity of the motor; B and J represent the coefficient of friction and moment of inertia, respectively; T_L and T_e represent load torque and electromagnetic torque, respectively; Δu_d, Δu_q, and ΔT_e are changes in u_d, u_q, and T_e, respectively.

The formulas for Δu_d, Δu_q, and ΔT_e are shown below:

$$\begin{cases} \Delta u_d = \Delta R_s i_d + \Delta L_d \dot{i}_d - \omega_e \Delta L_d i_q \\ \Delta u_q = \Delta R_s i_q + \Delta L_q \dot{i}_q + \omega_e (\Delta L_q i_d + \Delta \psi_m) \\ \Delta T_e = 1.5 p_n i_q [i_d (\Delta L_d - \Delta L_q) + \Delta \psi_m] \end{cases} \tag{2}$$

where ΔR_s and $\Delta \psi_m$ represent resistance and flux disturbance variables, respectively; ΔL_d and ΔL_q represent the d-q axis inductive disturbance variables, respectively.

In a single-input, single-output system, complex mathematical models can be written in the form of an ultra-local model

$$\begin{cases} \dot{x} = au + \tilde{G} \\ y = x \end{cases} \tag{3}$$

where x and u are the outputs and inputs of each loop, respectively. The controller gain is a. The uncertain variable of the ultra-local model is $\tilde{G}$.

In order to reduce the large error of uncertain variables in the ultra-local model, according to the new MFC theory, $\tilde{G}$ can be extended to obtain the ultra-local expansion model.

$$\begin{cases} \dot{x} = au + bx + G \\ y = x \end{cases} \tag{4}$$

where G is a nonlinear variable in the ultra-local expansion model. The linear function with respect to x is bx.

Using Eq. (4), the ultra-local expansion model of speed-current double closed loop is established:

$$\begin{cases} \dot{\omega}_e = a_\omega i_q - b_\omega \omega_e + G_\omega \\ \dot{i}_d = a_d u_d - b_d i_d + G_d \\ \dot{i}_q = a_q u_q - b_q i_q + G_q \end{cases} \tag{5}$$

The following matrix can be set:

$$\mathbf{a} = \begin{bmatrix} a_\omega & a_d & a_q \end{bmatrix}^T$$

$$= \begin{bmatrix} 1.5 p_n^2 [i_d (L_d - L_q) + \psi_m]/J & 1/L_d & 1/L_q \end{bmatrix}^T \tag{6}$$

$$\mathbf{b} = \begin{bmatrix} b_\omega & b_d & b_q \end{bmatrix}^T = \begin{bmatrix} B/J & -R_s/L_d & -R_s/L_q \end{bmatrix}^T \tag{7}$$

$$\mathbf{G} = \begin{bmatrix} G_\omega & G_d & G_q \end{bmatrix}^T = [\Delta T - p_n T_L/J$$

$$(\omega_e L_d i_q + \Delta u_d)/L_d \quad [\omega_e (L_q i_d + \psi_m) + \Delta u_q]/L_q]^T \tag{8}$$

According to Eqs. (6), (7), and (8), the speed-current loop ultra-local expansion model can be summarized as follows:

$$\dot{\mathbf{x}} = \mathbf{au} + \mathbf{bx} + \mathbf{G} \tag{9}$$

3. DUAL CLOSED-LOOP CONTROLLER DESIGN

3.1. MFSTTSMC Algorithm Design

Considering the influence of external load disturbance and internal motor parameter disturbance, in order to achieve the high-performance control requirements of the motor, the speed dynamic response is accelerated, and the transient performance

is improved. In this section, a super-twisting non-singular integral terminal sliding mode (STNITSM) is designed, and a model-free super-twisting terminal sliding mode controller (MFSTTSMC) algorithm based on speed-current double closed loop is designed by combining with new MFC algorithm. The structural block diagram of the MFSTTSMC involved in this paper is shown in Fig. 1.

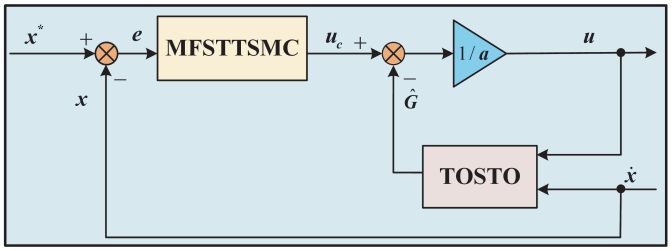

FIGURE 1. The framework of MFSTTSMC.

According to the new MFC algorithm and the speed-current ultra-local expansion model of Eq. (9), the controller of the system can be designed as:

$$\mathbf{u} = \frac{\dot{\mathbf{x}}^* - \mathbf{bx} - \mathbf{G} + \mathbf{u}_c}{\mathbf{a}} \tag{10}$$

where the elements in matrix $\mathbf{u} = [\ i_q^* \quad u_d^* \quad u_q^*\ ]^T$ represent the q-axis current output and the d-q axis voltage output of the system, respectively. The elements in matrix $\mathbf{x}^* = [\ \omega_e^* \quad i_d^* \quad i_q^*\ ]^T$ represent the specified values of system speed and the d-q axis current, respectively. The elements in matrix $\mathbf{x} = [\ \omega_e \quad i_d \quad i_q\ ]^T$ represent the system feedback values respectively. The elements in matrix $\mathbf{G} = [\ G_\omega \quad G_d \quad G_q\ ]^T$ are estimates of the nonlinear perturbation variables of the system. The element in matrix $\mathbf{u}_c = [\ u_{c\omega} \quad u_{cd} \quad u_{cq}\ ]^T$ is the output of the feedback controller.

Substituting Eq. (10) into Eq. (9) can derive Eq. (11):

$$\mathbf{u}_c = -(\dot{\mathbf{x}}^* - \dot{\mathbf{x}}) \tag{11}$$

Therefore, the errors of the system are defined as follows:

$$\mathbf{e} = [\ e_\omega \quad e_d \quad e_q\ ]^T = [\ \omega_e^* - \omega_e \quad i_d^* - i_d \quad i_q^* - i_q\ ]^T \tag{12}$$

The system state variables are defined as follows:

$$\begin{cases} \dot{\mathbf{e}}_1 = \mathbf{e}_2 \\ \dot{\mathbf{e}}_2 = \dot{\mathbf{e}} \end{cases} \tag{13}$$

The traditional speed loop MFSMC algorithm is established by the following Eq. (14).

$$\begin{cases} s_\omega = e_\omega + c\int e_\omega(\tau)\, d\tau \\ \dot{s}_\omega = -\varepsilon \mathrm{sign}(s_\omega) - k s_\omega \end{cases} \tag{14}$$

where $\varepsilon > 0$, $k > 0$, and $c > 0$. Since the MFSMC algorithm adopts the low-order sliding mode, the systematic error is very slow to converge. In order to make the state error converge in the global range, a high-order sliding mode STNITSM is designed.

Firstly, for the above Eq. (13) state variables, a non-singular integral terminal sliding mode (NITSM) based on double closed loop is designed:

$$\mathbf{s} = \dot{\mathbf{e}}_1 + \mathbf{k}\int \mathbf{e}_2^p \mathrm{sign}(\mathbf{e})\, \mathrm{d}\tau + \mathbf{c}\int e^{|e_2|}\mathrm{sign}(\mathbf{e})\, \mathrm{d}\tau \tag{15}$$

where the elements in $\mathbf{k}$ and $\mathbf{c}$ are both greater than zero, and the elements in $\mathbf{p}$ are positive odd numbers.

The derivative of Eq. (15) can be obtained:

$$\begin{aligned} \dot{\mathbf{s}} &= \ddot{\mathbf{e}}_1 + \mathbf{k}\mathbf{e}_2^p \mathrm{sign}(\mathbf{e}) + \mathbf{c}e^{|e_2|}\mathrm{sign}(\mathbf{e}) \\ &= \mathbf{k}\mathbf{e}_2^p \mathrm{sign}(\mathbf{e}) + \mathbf{c}e^{|e_2|}\mathrm{sign}(\mathbf{e}) - \mathbf{u}_c \end{aligned} \tag{16}$$

When $\dot{\mathbf{s}} = 0$, Eq. (16) can be written as:

$$-\dot{\mathbf{e}}_2 = \mathbf{u}_c = \mathbf{k}\mathbf{e}_2^p \mathrm{sign}(\mathbf{s}) + \mathbf{c}e^{|e_1|}\mathrm{sign}(\mathbf{s}) \tag{17}$$

Secondly, as a high-order sliding mode, the super-twisting sliding mode can effectively reduce the jitter phenomenon of the first-order linear sliding mode, and Eq. (18) gives the basic form of the super-twisting sliding mode algorithm.

$$\begin{cases} \dot{s}_\omega = -k_1 |s_\omega|^{1/2} \mathrm{sign}(s_\omega) + u_1 \\ \dot{u}_1 = -k_2 \mathrm{sign}(s_\omega) \end{cases} \tag{18}$$

where s_ω and u_1 are state variables. Both k_1 and k_2 are gain coefficients greater than zero. Since $|s_\omega|^{1/2}$ is calculated as a square root during the convergence process, the speed of error convergence is affected, affecting the transient performance of the motor.

Finally, to increase the response speed and transient performance of the system, an STNITSM algorithm is designed for the speed-current loop in combination with Eq. (15).

$$\begin{cases} \dot{\mathbf{s}} = -\mathbf{n}|\mathbf{s}|^{1/2}\mathrm{sign}(\mathbf{s}) - \mathbf{ms} + \mathbf{f} \\ \dot{\mathbf{f}} = -\boldsymbol{\alpha}\mathrm{sign}(\mathbf{s}) - \dot{\mathbf{G}} \\ \mathbf{s} = \mathbf{e}_2 + \mathbf{k}\int \mathbf{e}_2^p \mathrm{sign}(\mathbf{e})\, \mathrm{d}\tau + \mathbf{c}\int e^{|e_1|}\mathrm{sign}(\mathbf{e})\, \mathrm{d}\tau \end{cases} \tag{19}$$

where the elements in $\mathbf{n}$, $\mathbf{m}$, and $\boldsymbol{\alpha}$ are all greater than zero; $\mathbf{ms}$ is a fast term, and by combining the designed NITSM, the systematic error state can converge stably in a global range.

The feedback controller output is obtained by combining Eq. (16) and Eq. (19).

$$\begin{aligned} \mathbf{u}_c &= \mathbf{k}\mathbf{e}_2^p \mathrm{sign}(\mathbf{e}) + \mathbf{c}e^{|e_1|}\mathrm{sign}(\mathbf{e}) \\ &\quad + \mathbf{n}|\mathbf{s}|^{\frac{1}{2}}\mathrm{sign}(\mathbf{s}) + \mathbf{ms} + \alpha\int \mathrm{sign}(\mathbf{s}) \end{aligned} \tag{20}$$

Through Eq. (10) and Eq. (20), the MFSTTSMC control algorithm can be obtained:

$$\mathbf{u} = \frac{\begin{array}{c}\dot{\mathbf{x}}^* - \mathbf{bx} - \mathbf{G} + \mathbf{k}\mathbf{e}_2^p \mathrm{sign}(\mathbf{e}) + \mathbf{c}e^{|e_1|}\mathrm{sign}(\mathbf{e}) \\ + \mathbf{n}|\mathbf{s}|^{\frac{1}{2}}\mathrm{sign}(\mathbf{s}) + \mathbf{ms} + \boldsymbol{\alpha}\int \mathrm{sign}(\mathbf{s})\end{array}}{\mathbf{a}} \tag{21}$$

Next, the proof of stability is carried out.

Taking the speed controller as an example, the speed feedback output and controller output are shown below:

$$\begin{cases} u_{c\omega} = k_\omega e_2^{p_\omega} \text{sign}\left(e_\omega\right) + c_\omega e^{|e_{1\omega}|} \text{sign}\left(e_\omega\right) \\ +n_\omega \left|s_\omega\right|^{1/2} \text{sign}(s_\omega) + m_\omega s_\omega + \alpha_\omega \int \text{sign}(s_\omega) \\ i_q^* = \frac{\omega_e^* - b\omega_e - G_\omega + u_{c\omega}}{a_\omega} \end{cases} \tag{22}$$

Firstly, it is proved that the sliding surface converges and stabilizes in finite time. Choosing the Lyapunov function $V_\omega = e_{2\omega}^2/2$, its derivative can be obtained:

$$\begin{aligned} \dot{V}_\omega &= -e_{2\omega}\left[k e_{2\omega}^{p_\omega} \text{sign}\left(e_{2\omega}\right) + c e^{|e_{2\omega}|} \text{sign}\left(e_{2\omega}\right)\right] \\ &\le -\left[k e_{2\omega}^{p_\omega+1} + c e^{|e_{2\omega}|}\left|e_{2\omega}\right|\right] \end{aligned} \tag{23}$$

Since p_ω is positively odd, $\dot{V}_\omega \le 0$. The system error converges in time-limited according to the Lyapunov stability criterion. In the next step, it is proved that the designed STNITSM algorithm has a global stable convergence on NITSM.

Define the quadratic positive definite Lyapunov function as:

$$\begin{aligned} V_\omega\left(s_\omega, f_\omega\right) &= 2n_\omega \left|s_\omega\right| + \frac{1}{2} f_\omega^2 \\ &+\frac{1}{2}\left(\alpha_\omega \left|s_\omega\right|^{0.5} \text{sign}\left(s_\omega\right) - f_\omega\right)^2 \\ &= \frac{1}{2}\begin{bmatrix} \left|s_\omega\right|^{0.5} \text{sign}\left(s_\omega\right) \\ f_\omega \end{bmatrix}^T \begin{bmatrix} 4n_\omega + \alpha_\omega^2 & -\alpha_\omega \\ -\alpha_\omega & 2 \end{bmatrix} \\ &\begin{bmatrix} \left|s_\omega\right|^{0.5} \text{sign}\left(s_\omega\right) \\ f_\omega \end{bmatrix} \end{aligned} \tag{24}$$

Define the following formula:

$$\begin{cases} \boldsymbol{\zeta} = \begin{bmatrix} \left|s_\omega\right|^{0.5} \text{sign}\left(s_\omega\right) \\ f_\omega \end{bmatrix} \\ \mathbf{Q} = \begin{bmatrix} 4n_\omega + \alpha_\omega^2 & -\alpha_\omega \\ -\alpha_\omega & 2 \end{bmatrix} \end{cases} \tag{25}$$

Equation (24) can be simplified through Eq. (25) as:

$$V_\omega\left(s_\omega, f_\omega\right) = \boldsymbol{\zeta}^T \mathbf{Q} \boldsymbol{\zeta} \tag{26}$$

Using the equation $|\dot{s}_\omega| = \dot{s}_\omega \text{sign}(s_\omega)$, the equation for $\dot{\boldsymbol{\zeta}}$ can be given by:

$$\dot{\boldsymbol{\zeta}} = \frac{1}{\left|s_\omega\right|^{0.5}}\left(\mathbf{C} + \mathbf{D}\left|s_\omega\right|^{0.5} \dot{G}_\omega\right) \tag{27}$$

where $\mathbf{C} = \begin{bmatrix} -0.5n_\omega & 0.5 \\ -\alpha_\omega & 0 \end{bmatrix}$ and $\mathbf{D} = \begin{bmatrix} 0 & 1 \end{bmatrix}^T$. Suppose that $\dot{G}_\omega$ is bounded, $|\dot{G}_\omega| \le \delta$ and $\delta \in R^+$.

Combined with Eq. (27), the derivative of s is obtained:

$$\begin{aligned} \dot{V}_\omega(s_\omega, f_\omega) &= \frac{1}{\left|s_\omega\right|^{0.5}}\left(\boldsymbol{\zeta}^T \mathbf{C}^T \mathbf{Q} \boldsymbol{\zeta} + \boldsymbol{\zeta}^T \mathbf{Q}^T \mathbf{C} \boldsymbol{\zeta}\right. \\ &\left. + \left|s_\omega\right|^{0.5} \dot{G} \mathbf{D}^T \mathbf{Q} \boldsymbol{\zeta} + \left|s_\omega\right|^{0.5} \dot{G} \boldsymbol{\zeta}^T \mathbf{Q} \mathbf{D}^T\right) \\ &\le \frac{1}{\left|s_\omega\right|^{0.5}} \boldsymbol{\zeta}^T \left(\mathbf{C}^T \mathbf{Q} + \mathbf{Q}\mathbf{C} + \delta^2 \mathbf{E}^T \mathbf{E} + \mathbf{Q}\mathbf{D}\mathbf{D}^T\right) \boldsymbol{\zeta} \\ &= \frac{1}{\left|s_\omega\right|^{0.5}} \boldsymbol{\zeta}^T \mathbf{F} \boldsymbol{\zeta} \end{aligned} \tag{28}$$

where $\mathbf{E} = \begin{bmatrix} 1 & 0 \end{bmatrix}$ and $\mathbf{F} = -\mathbf{C}^T\mathbf{Q} + \mathbf{Q}\mathbf{C} + \delta^2 \mathbf{E}^T \mathbf{E} + \mathbf{Q}\mathbf{D}\mathbf{D}^T$.

Therefore, it can be seen that $\dot{V}_\omega(s_\omega, f_\omega) < 0$ and $V_\omega(s_\omega, f_\omega) > 0$ satisfy the stability condition of the quadratic Lyapunov function.

Matrix $\mathbf{F}$ is shown below:

$$\mathbf{F} = \begin{bmatrix} n_\omega \alpha_\omega + \frac{n_\omega^3}{2} - \delta^2 - \frac{n_\omega^2}{2} & \frac{n_\omega}{2} - \frac{n_\omega^2}{2} \\ \frac{n_\omega}{2} - \frac{n_\omega^2}{2} & \frac{n_\omega}{2} - 1 \end{bmatrix} \tag{29}$$

From Eq. (29), the matrix $\mathbf{Q}$ and matrix $\mathbf{F}$ can be obtained, and the conditions for symmetric positive definite matrices are as follows:

$$\begin{cases} n_\omega > 2 \\ \alpha_\omega > \frac{n_\omega^3 + \delta^2(4n_\omega - 8)}{n_\omega(4n_\omega - 8)} \end{cases} \tag{30}$$

The stability of the speed controller is proved, and the same is true for the stability of the current controller. Therefore, according to the above proof, it can be seen that the control system based on speed-current double closed-loop MFSTTSMC has stable convergence in the global range.

3.2. Third-Order Super-Twisting Observation Algorithm

In order to have a better observation effect on the nonlinear variables in the ultra-local extended model in this paper, according to the formula of the ultra-local extended model in Eq. (11), the following conventional super-twisting observer (STO) based on the rotational speed loop is designed:

$$\begin{cases} \dot{\omega}_e^* = a_\omega i_q^* + b_\omega \omega_e + \hat{G}_\omega \\ \dot{\hat{G}}_\omega = -k_1 \left|s_{o\omega}\right|^{\frac{1}{2}} \text{sign}(s) - \int k_2 \text{sign}(s_{o\omega}) \end{cases} \tag{31}$$

where the observed value of motor speed is $\hat{\omega}_e$; $\hat{G}_\omega$ is the real-time observation of the nonlinear disturbance of the rotational speed system. $s_{o\omega}$ is the sliding mode, $s_{o\omega} = \omega_e - \hat{\omega}_e$.

Due to the slow dynamic response of traditional STO, the estimation of perturbation feedback is delayed, which affects the observation accuracy. In order to improve the dynamic response speed and observation accuracy, a third-order super-twisting observer (TOSTO) based on rotational speed-current double closed-loop is proposed:

$$\begin{cases} \dot{\hat{\mathbf{x}}} = \mathbf{au} + \mathbf{bx} + \hat{\mathbf{G}} \\ \hat{\mathbf{G}} = \mathbf{vU} \end{cases} \tag{32}$$

where the elements in $\mathbf{v}$ are all greater than zero. $\hat{\mathbf{G}}$ is the perturbation observation matrix, and $\hat{\mathbf{G}} = \begin{bmatrix} \hat{G}_\omega & \hat{G}_d & \hat{G}_q \end{bmatrix}^T$. $\mathbf{U}$

is a matrix of third-order super-twisting functions, and $\mathbf{U} = \begin{bmatrix} U_\omega & U_d & U_q \end{bmatrix}^T$.

The matrix expression of the TOSTO function is designed as follows:

$$\begin{cases} \dot{\mathbf{U}} = \mathbf{U}_1 \\ \dot{\mathbf{U}}_1 = \mathbf{U}_2 - \mathbf{r}_2|\mathbf{e}|^{1/2}\text{sign}(\mathbf{e}) + \mathbf{r}_1\mathbf{e} \\ \dot{\mathbf{U}}_2 = -\mathbf{r}_3|\mathbf{e}|\text{sign}(\mathbf{e}) + \dot{\mathbf{g}} \\ |\mathbf{e}| = \mathbf{U}_1 = \mathbf{x} - \hat{\mathbf{x}} \end{cases} \tag{33}$$

where the elements $\mathbf{r}_1$, $\mathbf{r}_2$, and $\mathbf{r}$ are all greater than zero. The elements in $\mathbf{g}$ are nonlinear perturbation variables, and $\mathbf{g} = \begin{bmatrix} g_\omega & g_d & g_q \end{bmatrix}$.

The speed-current double closed-loop MFSTTSMC based on the TOSTO is designed as follows:

$$\mathbf{u} = \frac{\dot{\mathbf{x}}^* - \mathbf{b}\mathbf{x} - \mathbf{v}\mathbf{U} + \mathbf{u}_c}{\mathbf{a}} \tag{34}$$

Taking the speed loop as an example, the TOSTO based on the speed loop is designed as follows:

$$\begin{cases} \dot{U}_\omega = U_{1\omega} \\ \dot{U}_{1\omega} = U_{2\omega} - r_{2\omega}|e_\omega|^{1/2}\text{sign}(e_\omega) + r_{1\omega}e_\omega \\ \dot{U}_{2\omega} = -r_{3\omega}|e_\omega|\text{sign}(e_\omega) + \dot{g}_\omega \\ e_\omega = U_{1\omega} = \dot{\omega}_e - \dot{\hat{\omega}}_e \end{cases} \tag{35}$$

The rotation speed loop output controller is designed:

$$i_q = \frac{\omega_e^* - b_\omega\omega_e - v_\omega U_\omega + u_{c\omega}}{a_\omega} \tag{36}$$

The next step will be to perform a proof of stability of the rotation loop system, using the Lyapunov function V_ω:

$$V_\omega = \mathbf{\Gamma}^T\mathbf{J}\mathbf{\Gamma} \tag{37}$$

where $\mathbf{\Gamma}^T = \begin{bmatrix} |e_\omega|^{1/2}\text{sign}(e_\omega) & e_\omega & U_{2\omega} \end{bmatrix}$; $\mathbf{J} = \frac{1}{2}\begin{bmatrix} 4r_{3\omega} + r_{2\omega}^2 & -r_{1\omega}r_{2\omega} & -r_{2\omega} \\ -r_{1\omega}r_{2\omega} & r_{1\omega}^2 & r_{1\omega 23} \\ -r_{2\omega} & r_{1\omega} & 2 \end{bmatrix}$, and $\mathbf{J}$ is a positive definite matrix.

According to Eq. (37), Eq. (38) can be obtained as follows:

$$\lambda_{\min}(\mathbf{J})\|\mathbf{\Gamma}\|^2 < V_\omega < \lambda_{\max}(\mathbf{J})\|\mathbf{\Gamma}\|^2 \tag{38}$$

where $\lambda_{\max}(\mathbf{J})$ is the maximum eigenvalue of matrix $\mathbf{J}$. $\lambda_{\min}(\mathbf{J})$ is the minimum eigenvalue of matrix $\mathbf{J}$.

According to the quadratic standard inequality, the following equation can be derived:

$$\begin{cases} |e_\omega|^{1/2} \le \|\mathbf{\Gamma}\| \le V_\omega^{1/2}/\lambda_{\min}(\mathbf{J}) \\ \|\mathbf{\Gamma}\| = \sqrt{|e_\omega| + e_\omega^2 + U_{2\omega}^2} \end{cases} \tag{39}$$

The derivative of $\mathbf{\Gamma}$ is obtained:

$$\begin{aligned} \dot{\mathbf{\Gamma}} &= \begin{bmatrix} \frac{1}{2}\frac{1}{|e_\omega|^{1/2}}\dot{e}_\omega \\ \dot{e}_\omega \\ \dot{U}_{2\omega} \end{bmatrix} \\ &= \begin{bmatrix} \frac{1}{2}\frac{1}{|e_\omega|^{1/2}}\left(-r_{2\omega}|e_\omega|^{1/2}\text{sign}(e_\omega) + r_{1\omega} + U_{2\omega}\right) \\ -r_{2\omega}|e_\omega|^{1/2}\text{sign}(e_\omega) + r_{1\omega} + U_{2\omega} \\ \dot{g} - r_{3\omega}\text{sign}(e_\omega) \end{bmatrix} \\ &= \frac{1}{|e_\omega|^{1/2}}\mathbf{P}_1\mathbf{\Gamma} + \mathbf{P}_2\dot{\mathbf{\Gamma}} + \boldsymbol{\eta} \end{aligned} \tag{40}$$

where $\mathbf{P}_1 = \frac{1}{2}\begin{bmatrix} -r_{2\omega} & r_{1\omega} & 1 \\ 0 & 0 & 0 \\ -2r_{3\omega} & 0 & 0 \end{bmatrix}$; $\mathbf{P}_2 = \begin{bmatrix} 0 & 0 & 1 \\ -r_{2\omega} & r_{1\omega} & 1 \\ 0 & 0 & 0 \end{bmatrix}$; $\boldsymbol{\eta}^T = \begin{bmatrix} 0 & 0 & \dot{g}_\omega \end{bmatrix}^T$.

The derivative of V_ω is obtained:

$$\begin{aligned} \dot{V}_\omega &= \frac{1}{|e_\omega|^{1/2}}\mathbf{\Gamma}^T\left[\mathbf{P}_1^T\mathbf{J} + \mathbf{J}\mathbf{P}_1\right]\mathbf{\Gamma} \\ &\quad + \mathbf{\Gamma}^T\left[\mathbf{P}_2^T\mathbf{J} + \mathbf{J}\mathbf{P}_2\right]\mathbf{\Gamma} + \boldsymbol{\eta}^T\mathbf{J}\mathbf{\Gamma} + \mathbf{\Gamma}^T(\mathbf{J}\boldsymbol{\eta}) \\ &= -\frac{1}{|e_\omega|^{1/2}}\mathbf{\Gamma}^T\mathbf{q}_1\mathbf{\Gamma} - \mathbf{\Gamma}^T\mathbf{q}_2\mathbf{\Gamma} + \dot{g}\mathbf{q}_3^T\mathbf{\Gamma} \end{aligned} \tag{41}$$

where $\mathbf{q}_1 = \frac{1}{2}\begin{bmatrix} 2r_{2\omega}r_{3\omega} + r_{2\omega}^2 & \left(r_{2\omega}^2 + r_{3\omega}\right)r_{1\omega} & r_{2\omega}^2 \\ \left(r_{2\omega}^2 + r_{3\omega}\right)r_{1\omega} & -r_{2\omega}r_{1\omega}^2 & -r_{2\omega}r_{1\omega} \\ r_{2\omega}^2 & -r_{2\omega}r_{1\omega} & -r_{2\omega} \end{bmatrix}$;

$\mathbf{q}_2 = r_{1\omega}\begin{bmatrix} r_{2\omega}^2 & -r_{2\omega}r_{1\omega} & -r_{2\omega} \\ -r_{2\omega}r_{1\omega} & r_{1\omega}^2 & r_{1\omega} \\ -r_{2\omega} & r_{1\omega} & 1 \end{bmatrix}$; $\mathbf{q}_3 = \begin{bmatrix} -r_{2\omega} & r_{1\omega} & 2 \end{bmatrix}$.

It is assumed that perturbation variable g_ω is bounded, $g_\omega \le \sigma$ and $\sigma \in R$. Eq. (41) can be rewritten:

$$\begin{aligned} \dot{V}_\omega &= -\frac{1}{|e_\omega|^{1/2}}\mathbf{\Gamma}^T\mathbf{q}_1\mathbf{\Gamma} - \mathbf{\Gamma}^T\mathbf{q}_2\mathbf{\Gamma} + \dot{g}\mathbf{q}_3^T\mathbf{\Gamma} \\ &\le -\frac{1}{|e_\omega|^{1/2}}\mathbf{\Gamma}^T\mathbf{q}_1\mathbf{\Gamma} - \mathbf{\Gamma}^T\mathbf{q}_2\mathbf{\Gamma} + \sigma\mathbf{q}_3^T\mathbf{\Gamma} \end{aligned} \tag{42}$$

In Eq. (41), $\dot{g}\mathbf{q}_3^T\mathbf{\Gamma}$ can be further simplified:

$$\begin{aligned} \dot{g}\mathbf{q}_3^T\mathbf{\Gamma} &= \frac{\dot{g}}{|e_\omega|^{1/2}}\left[-r_{2\omega}|e_\omega|^{1/2}\text{sign}(e_\omega)\right. \\ &\quad \left. + r_{1\omega}e_\omega|e_\omega|^{1/2} + 2U_{2\omega}|e_\omega|^{1/2}\right] \\ &= \frac{1}{|e_\omega|^{1/2}}\mathbf{\Gamma}^T\mathbf{L}_1\mathbf{\Gamma} + \mathbf{\Gamma}^T\mathbf{L}_2\mathbf{\Gamma} \end{aligned} \tag{43}$$

where $\mathbf{L}_1 = \begin{bmatrix} -r_{2\omega}\dot{g}_\omega\text{sign}(e_\omega) & 0 & \dot{g}_\omega\text{sign}(e_\omega) \\ 0 & r_{1\omega}\dot{g}_\omega & 0 \\ \dot{g}_\omega\text{sign}(e_\omega) & 0 & 0 \end{bmatrix}$;

$\mathbf{L}_2 = \begin{bmatrix} -r_{1\omega}\dot{g}_\omega\text{sign}(e_\omega) & 0 & 0 \\ 0 & 0 & 0 \\ 0 & 0 & 0 \end{bmatrix}$.

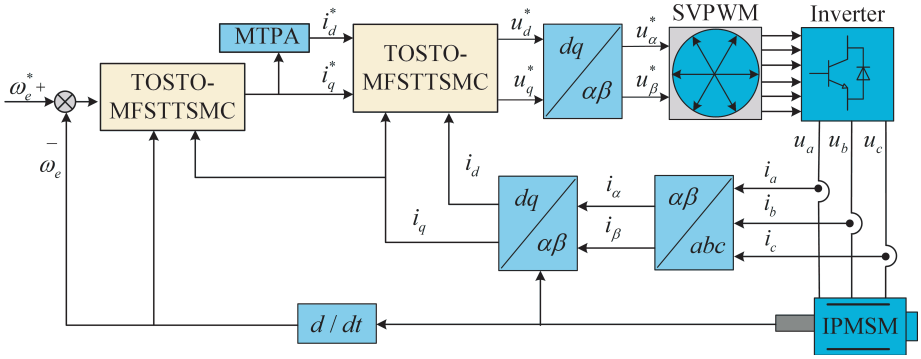

FIGURE 2. The framework of the TOSTO-MFSTTSMC algorithm.

Substituting Eq. (43) into Eq. (41), Eq. (44) can be obtained as follows:

$$\begin{aligned}\dot{V}_\omega &= -\frac{1}{|e_\omega|^{1/2}}\mathbf{\Gamma}^T\mathbf{q}_1\mathbf{\Gamma} - \mathbf{\Gamma}^T\mathbf{q}_2\mathbf{\Gamma} + \dot{g}\mathbf{q}_3^T\mathbf{\Gamma} \\ &= -\frac{1}{|e_\omega|^{1/2}}\mathbf{\Gamma}^T\left(\mathbf{q}_1 - \mathbf{L}_1\right)\mathbf{\Gamma} - \mathbf{\Gamma}^T\left(\mathbf{q}_2 - \mathbf{L}_2\right)\mathbf{\Gamma} \end{aligned} \quad (44)$$

From Eq. (44) it can be seen that in order for $\dot{V}_\omega < 0$, the following conditions need to be met.

$$\begin{cases} \mathbf{q}_1 - \mathbf{L}_1 > 0 \\ \mathbf{q}_2 - \mathbf{L}_2 > 0 \end{cases} \quad (45)$$

Eq. (45) can be further simplified:

$$\begin{cases} r_{2\omega}^2 + 2r_{3\omega} + 2\dot{g}_\omega \text{sign}\left(e_\omega\right) > 0 \\ r_{1\omega}^2 r_{3\omega}^2 - 2r_{1\omega}^2 r_{2\omega}^2 \dot{g}_\omega \text{sign}\left(e_\omega\right) > 0 \\ r_{1\omega}^2 r_{2\omega}\left(r_{3\omega} + 2\dot{g}_\omega \text{sign}\left(e_\omega\right)\right)^2 > 0 \\ 2r_{2\omega}^2 + \dot{g}_\omega \text{sign}\left(e_\omega\right) > 0 \\ r_{2\omega}^2 + \dot{g}_\omega \text{sign}\left(e_\omega\right) - r_{1\omega} r_{2\omega}^2 > 0 \end{cases} \quad (46)$$

According to Eq. (38), Eq. (39) and the conditions that satisfy Eq. (46), $\dot{V}_\omega$ can be obtained:

$$\begin{aligned}\dot{V}_\omega &= -\frac{1}{|e_\omega|^{1/2}}\mathbf{\Gamma}^T\left(\mathbf{q}_1 - \mathbf{L}_1\right)\mathbf{\Gamma} - \mathbf{\Gamma}^T\left(\mathbf{q}_2 - \mathbf{L}_2\right)\mathbf{\Gamma} \\ &\le -\frac{\lambda_{\min}^{1/2}\left(\mathbf{J}\right)\sigma\left(\mathbf{q}_1 - \mathbf{L}_1\right)}{\lambda_{\max}^{1/2}\left(\mathbf{J}\right)} V_\omega^{1/2} - \frac{\lambda_{\min}^{1/2}\left(\mathbf{J}\right)\left(\mathbf{q}_2 - \mathbf{L}_2\right)}{\lambda_{\max}^{1/2}\left(\mathbf{J}\right)} V_\omega^{1/2} \\ &\le -\frac{\lambda_{\min}^{1/2}\left(\mathbf{J}\right)\sigma\left(\mathbf{q}_1 - \mathbf{L}_1\right)}{\lambda_{\max}^{1/2}\left(\mathbf{J}\right)} V_\omega^{1/2} \le 0 \end{aligned} \quad (47)$$

According to $\dot{V}_\omega \le 0$, the systematic error will converge in a finite time. The speed loop observer is proven, and the same is true for the current loop observer.

4. SIMULATION AND EXPERIMENTATION

4.1. Simulation Results and Analysis

Figure 2 shows the framework of the TOSTO-MFSTTSMC algorithm-driven system proposed in this paper. As can be seen in Fig. 2, the MFSTTSMC control algorithm is used for the speed-current double closed loop, and the nonlinear variables in the ultra-local expansion model are accurately estimated by TOSTO to achieve feedforward compensation, so as to improve the response speed and transient performance of IPMSM. The motor model of the proposed control algorithm is built by using the MATLAB platform, and the data were compared with the MFSMC and STO-MFSMC. The parameters of the motor are shown in Table 1. The three controller parameters are shown in Table 2.

TABLE 1. The Parameters of The Motor.

Parameter	Unit	Values
voltage/u_{dc}	V	311
current/I_N	A	21
Stator resistance/R_s	Ω	0.04
q-axis inductance/L_q	H	0.334
d-axis inductance/L_d	H	0.25
Pole number/p_n	pairs	4
Magnetic flux/ψ_m	Wb	0.081
Inertia/J	kg · m^2	0.003
Damping factor/B	Nm · s/rad	0.008

Set the specified speed at the initial point a to 1000 r/min, and the starting load torque to 10 N · m. At point b 0.3 s, the specified speed is 1500 r/min. At point c 0.6 s, the load is increased to 20 N · m. At point d 0.9 s, the full load is removed. At point e 1.2 s, the flux 0.081 Wb is reduced to 0.04 Wb. At point f point 1.4 s, the stator resistance increases from 0.04 Ω to 0.1 Ω. At point g 1.6 s, L_q increases from 0.334 mH to 0.8 mH. At point h 1.8 s, L_d increases from 0.25 mH to 0.5 mH.

Figure 3 illustrates the full operating conditions of the motor under external load disturbances and internal parameter mismatch. It can be seen from the external disturbance operation conditions in Fig. 3(a) and the internal parameter disturbance operating conditions in Fig. 3(b) that the TOSTO-MFSTTSMC

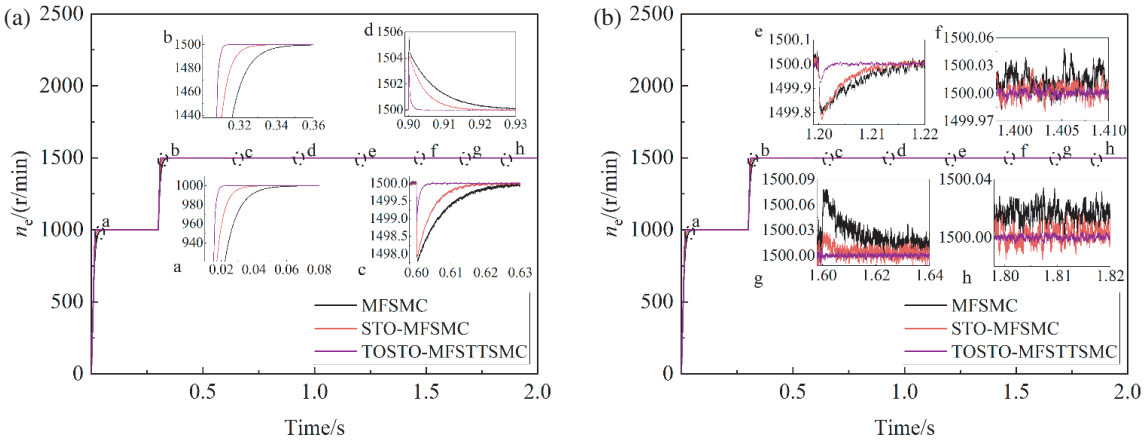

FIGURE 3. Waveforms of motors operating under complex conditions. (a) External disturbances. (b) Internal parameter perturbations.

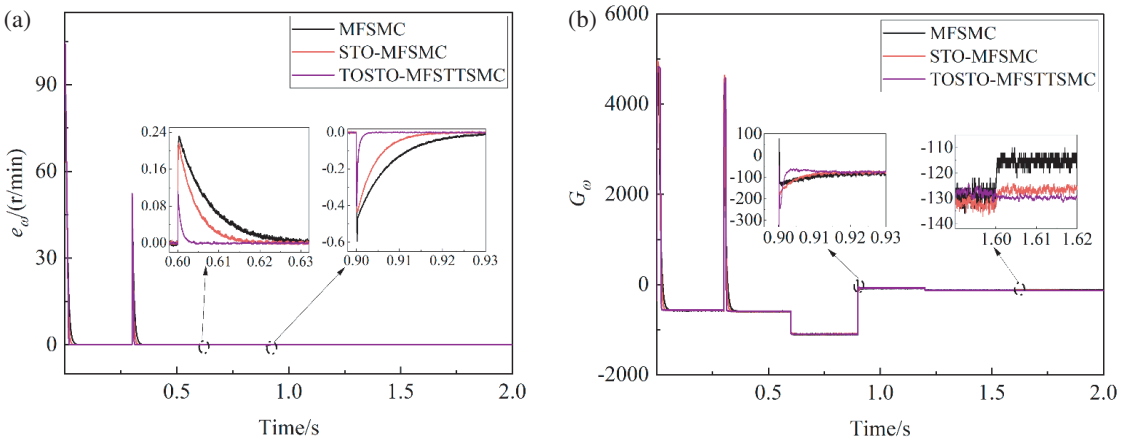

FIGURE 4. Comparison of observer performance. (a) RPM observation error. (b) Observed disturbances G_ω.

TABLE 2. The three controller parameters.

Control algorithms	The speed controller	The current controller
MFSMC	$c = 300, \varepsilon = 200, k = 0.1$	$k_I = 50, k_p = 80$
STO-MFSMC	$c = 280, \varepsilon = 140, k = 0.2$ $k_1 = 0.3, k_2 = 400$	$k_I = 50, k_p = 80$
TOSTO-MFSTTSMC	$k_\omega = 100, c_\omega = 10, n_\omega = 0.2$	$k = 60, c = 600, n = 0.2$
	$m_\omega = 300, \alpha_\omega = 0.2, r_{1\omega} = 0.8$	$m = 300, \alpha = 0.1, r = 0.8$
	$r_{2\omega} = 2, r_{3\omega} = 1, v_\omega = 866, p_\omega = 1.2$	$r_2 = 2, r_3 = 1, v = 300, p = 1.5$

algorithm has better transient performance than the MFSMC and STO-MFSMC algorithms. At point a, the MFSMC and STO-MFSMC algorithms take 0.69 s and 0.48 s respectively to make the motor output to the specified value, while the TOSTO-MFSTTSMC algorithm only uses 0.23 s. Compared with the first two algorithms, the response speed and transient performance of TOSTO-MFSTTSMC have been greatly improved.

Figure 4 shows a comparison of the overall the performance of the observers. As can be seen from Fig. 4(a) and Fig. 4(b), the tosto-MFSTTSMC has a smaller steady-state error of rotational speed than the MFSMC and STO-MFSMC, and can be quickly and accurately traced to a given value. Therefore, the TOSTO-MFSTTSMC algorithm can weaken the high-frequency harmonics of the rotational speed to a certain extent.

Figure 5 shows the full operating condition simulation of the motor parameters, and Figs. 5(a), 5(b), and 5(c) are the d-axis current, q-axis current, and electromagnetic torque, respectively. Because the observation accuracy of the TOSTO-MFSTTSMC algorithm is superior to that of the MFSMC and STO-MFSMC algorithms, the current pulsation and electromagnetic torque pulsation of the d-q axis are effectively weakened.

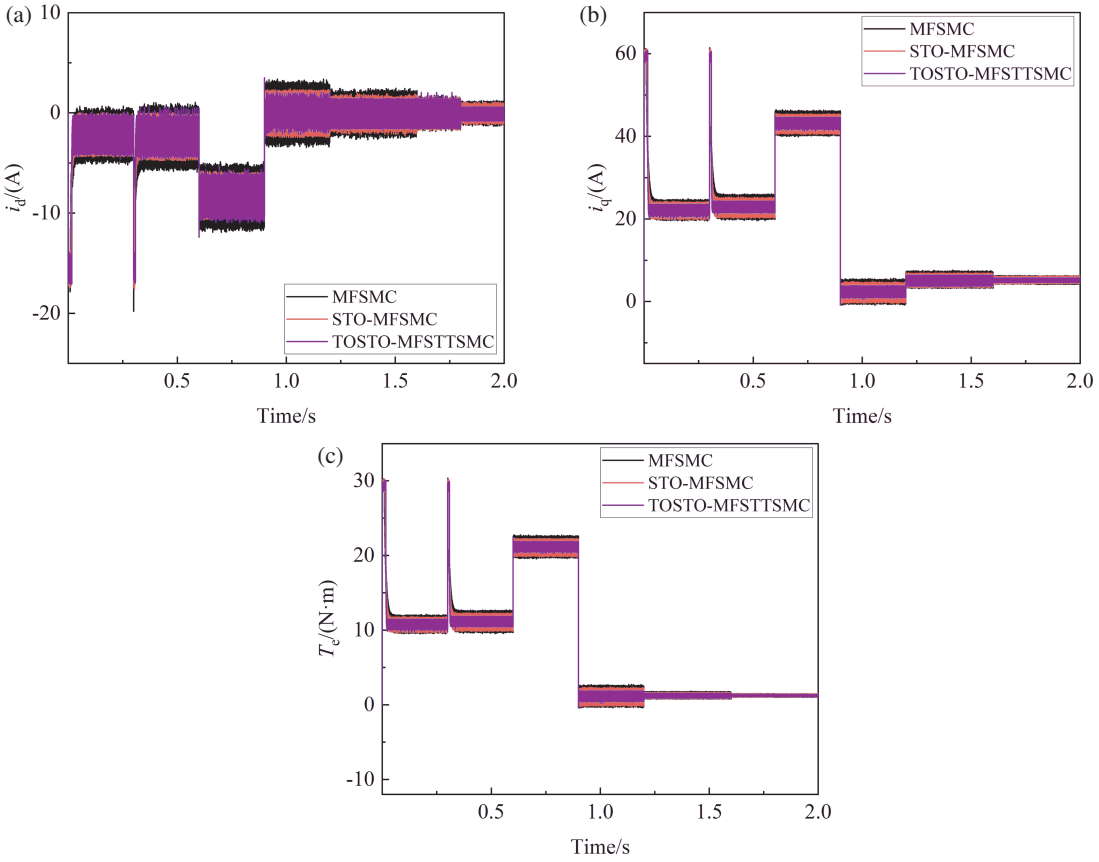

FIGURE 5. Waveforms of motor parameters under full working conditions. (a) *d*-axis current. (b) *q*-axis current. (c) Electromagnetic torque.

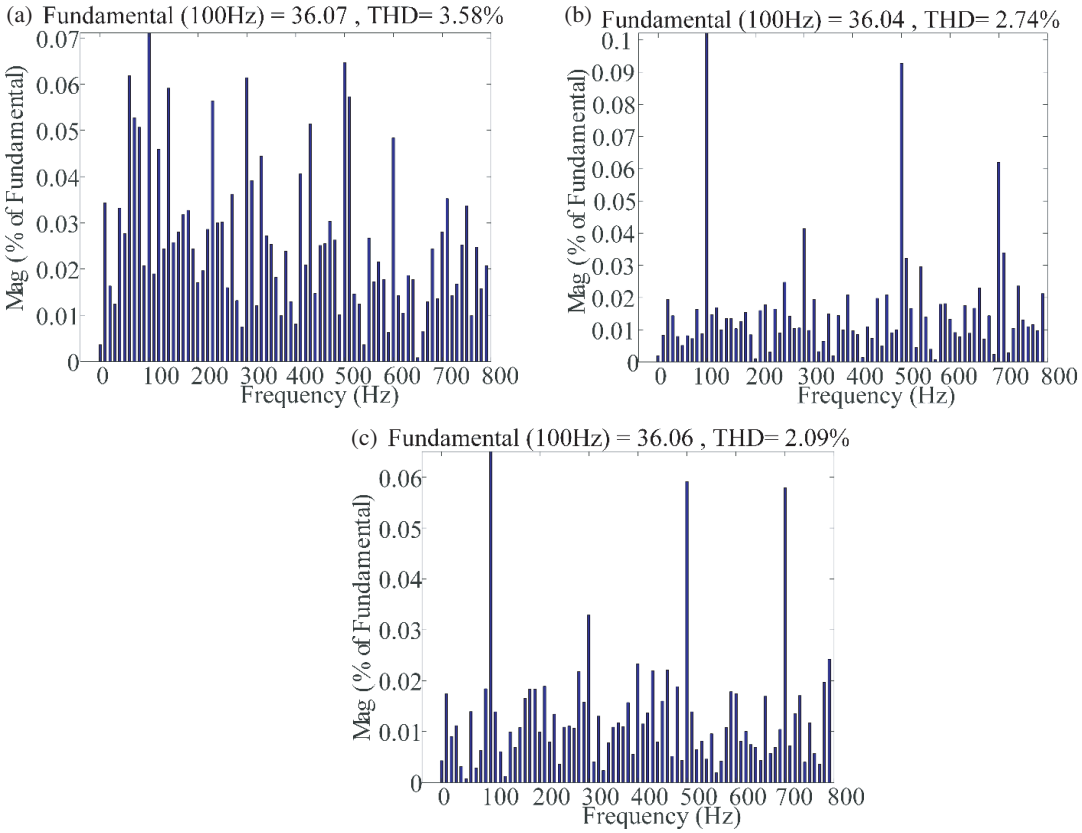

FIGURE 6. THD analysis of a-phase current at 0.8 s for three control algorithms. (a) MFSMC. (b) STO-MFSMC. (c) TOSTO-MFSTTSMC.

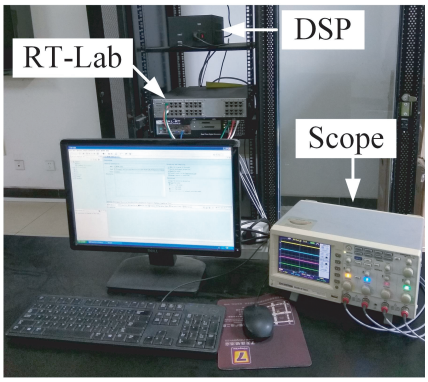

FIGURE 7. RT-LAB experimental platform.

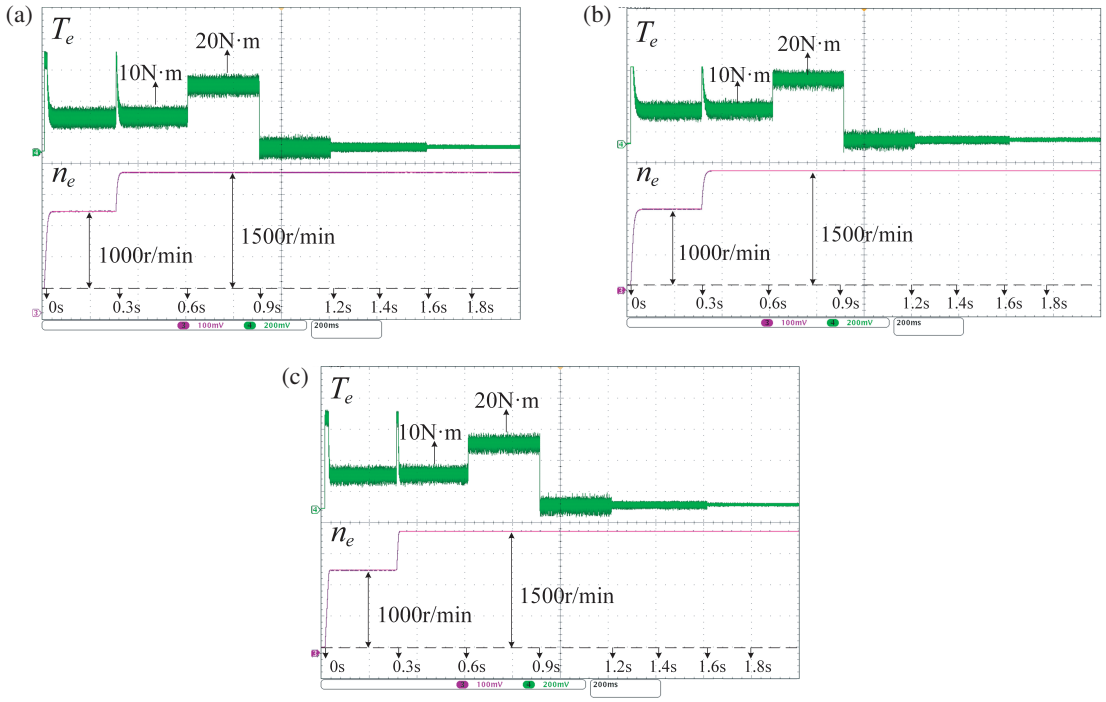

FIGURE 8. Experimental waveform of RPM-torque. (a) MFSMC. (b) STO-MFSMC. (c) TOSTO-MFSTTSMC.

Figure 6 shows the THD analysis of a-phase current at 0.8 s for three control algorithms. As can be seen from Fig. 6, the THDs of MFSMC and STO-MFSMC are 3.58% and 2.74%, respectively. The control algorithm proposed in this paper can make the systematic error converge quickly and stably in the global world, and effectively weaken the high-frequency harmonics. Therefore, the THD of the TOSTO-MFSTTSMC algorithm is only 2.09%.

4.2. Experimental Results and Analysis

Hardware-in-the-loop simulation experiments were performed on an RT-LAB platform, and Fig. 7 shows the RT-LAB experimental platform. The experimental parameters and experimental conditions are the same as those of MATLAB simulation.

Figures 8 and 9 show the speed-torque experimental waveform and d-q current experimental waveform, respectively. As can be seen from Fig. 8 and Fig. 9, the time required for the system to converge to stability at initial startup is 0.69 seconds and 0.48 seconds under the MFSMC and STO-MFSMC control algorithms, respectively. The observation error of MFSMC and STO-MFSMC is large, and the torque pulsation is 15% and 11%, respectively. The double-closed-loop TOSTO-MFSTTSMC control algorithm proposed in this paper makes the systematic error converge quickly and stably globally through the designed MFSTTSMC algorithm, and only 0.23 s is required to make the output quickly converge to be stable at the initial start-up. In addition, the designed TOSTO algorithm improves the dynamic response speed and observation accuracy of the observer, so that the torque pulsation is only 6.5%.

Figures 10 and 11 show the experimental waveform of phase A current under all operating conditions and the experimental waveform of phase A current in the period of 0.8 s–1.5 s,

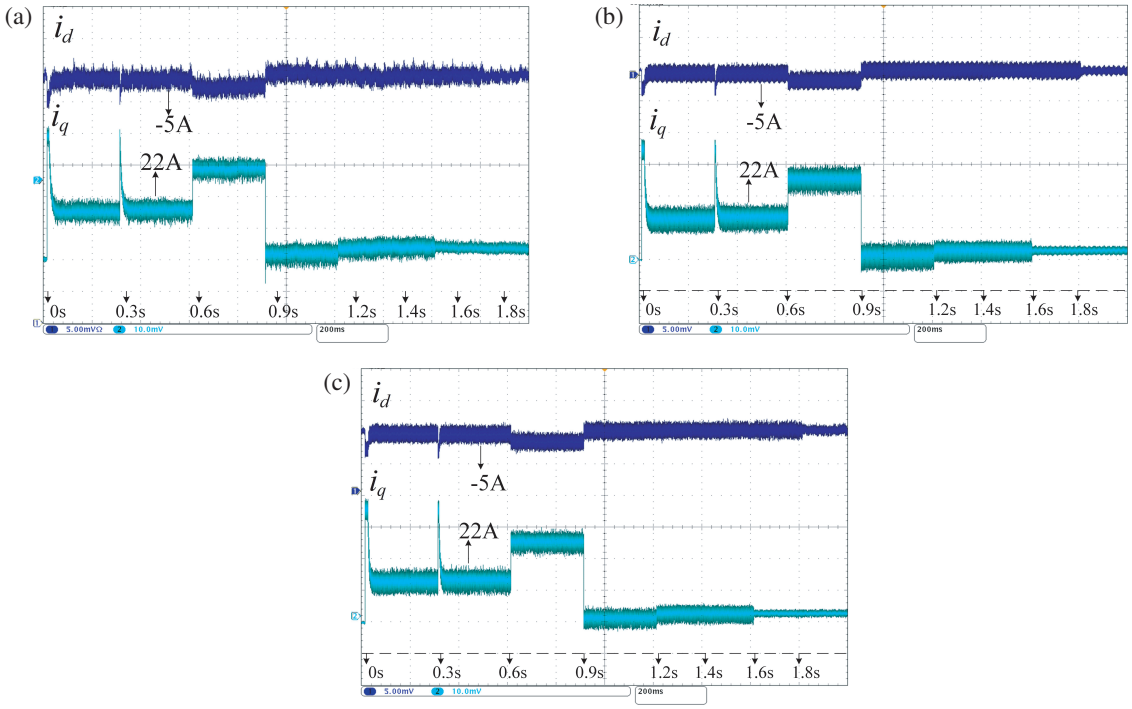

FIGURE 9. Experimental waveform of *d*-*q* axis current. (a) MFSMC. (b) STO-MFSMC. (c) TOSTO-MFSTTSMC.

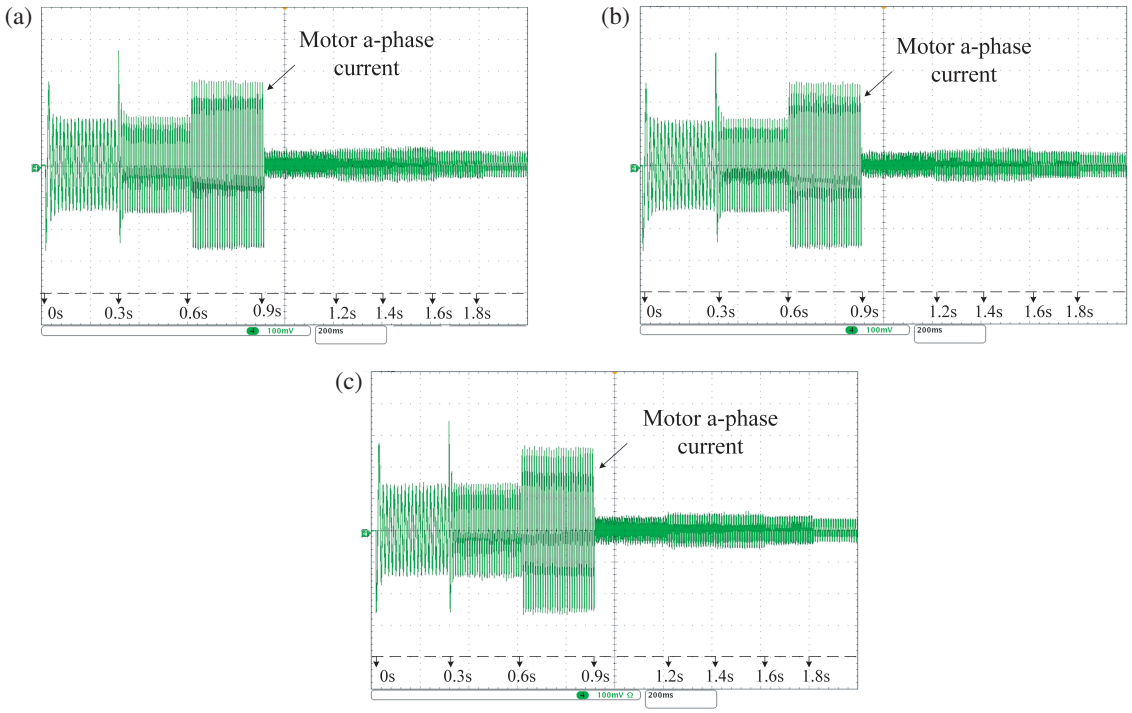

FIGURE 10. Experimental waveforms of a-phase current at full working conditions. (a) MFSMC. (b) STO-MFSMC. (c) TOSTO-MFSTTSMC.

respectively. Compared with MFSMC and STO-MFSMC, the double-closed-loop TOSTO-MFSTTSMC control algorithm proposed in this paper can accelerate the systematic error convergence speed and improve the dynamic response ability and observation accuracy. As can be seen from Figs. 10 and 11, the TOSTO-MFSTTSMC control algorithm is faster than the first two control algorithms, and the current waveform is relatively smooth.

Table 3 shows the comparison of the overall performance of the three control algorithms. From the comparison of various performance indexes in Table 3, it is obvious that the control algorithm proposed in this paper is better than the first two control

TABLE 3. The overall performance comparison of control algorithms.

Parameters	MFSMC	STO-MFSMC	TOSTO-MFSTTSMC
Initial convergence time (s)	0.69	0.48	0.23
Torque pulsation (%)	15	11	6.5
a Phase current THD (%)	3.58	2.74	2.09

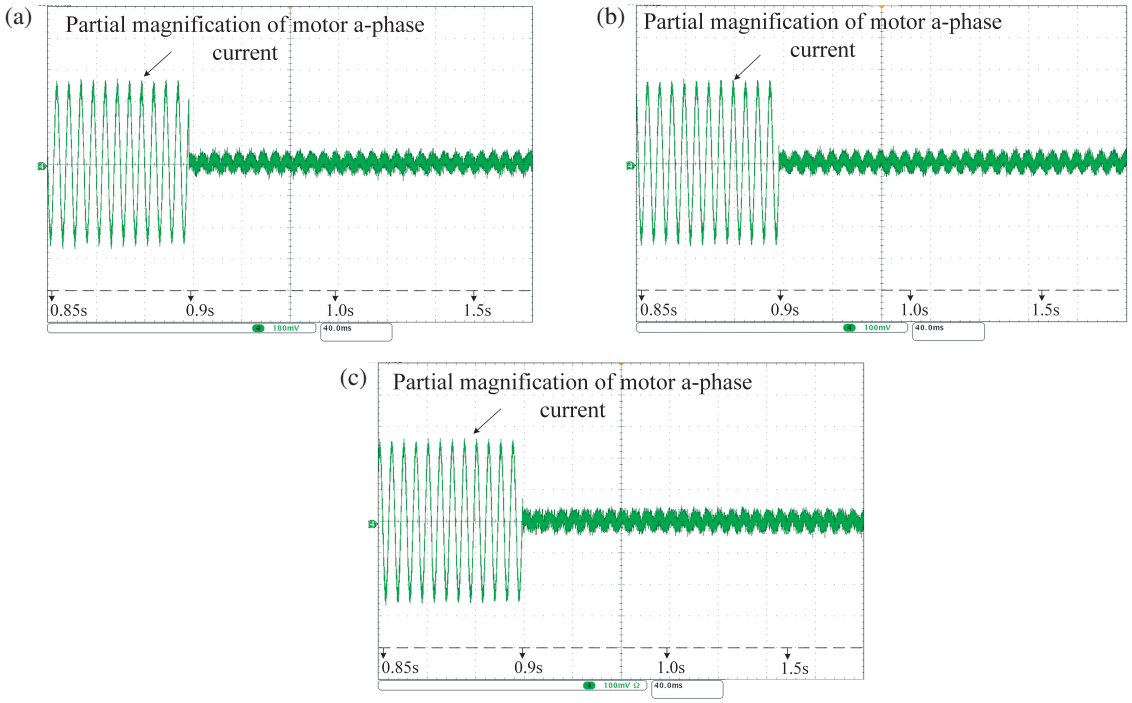

FIGURE 11. Experimental waveform of a-phase current under 0.8 s–1.5 s time period.

methods in terms of system response speed, current THD value, and torque pulsation.

5. CONCLUSION

To solve the problem of poor control performance of IPMSM due to parameter perturbations and external perturbations when adopting MFSMC algorithm, a double-closed-loop MF-STTSMC algorithm of IPMSM based on TOSTO is proposed. The algorithm proposed in this paper can realize the rapid and stable convergence of systematic error variables in the global world, improve the transient performance, and enhance the robustness of the system. Through the simulation and analysis of experimental results under complex working conditions, the following conclusions are drawn:

(1) In this paper, a double-closed-loop MFSTTSMC control algorithm is designed based on the new MFC algorithm. Through the design of STNITSM, the systematic error converges quickly and stably in the global world, and the convergence time is only 0.23 s at the initial start-up, which has a good dynamic response ability.

(2) For the nonlinear perturbation variables in the ultra-local extension model, a TOSTO algorithm is designed. The TOSTO algorithm improved observer is designed to enhance the dynamic response ability and observation accuracy of the observer, and effectively weaken the torque and current pulsation.

(3) Compared with the MFSMC and STO-MFSMC algorithms, the double-closed-loop TOSTO-MFSTTSMC algorithm proposed in this paper reduces the torque pulsation and a-phase current THD to 6.5% and 2.09%, respectively, which enhances the transient performance of the motor and makes the overall performance of the motor superior.

ACKNOWLEDGEMENT

This work was supported by the Scientific Research Fund of Hunan Provincial Education Department under Grant Number 23B1017.

REFERENCES

[1] Shen, J., X. Wang, D. Xiao, Z. Wang, Y. Mao, and M. He, "Online switching strategy between dual three-phase PMSM and open-winding PMSM," *IEEE Transactions on Transportation Electrification*, Vol. 10, No. 1, 1519–1529, Mar. 2024.

[2] Wang, H., M. Fan, Y. Xiao, Y. Yang, Z. Dai, X. Zhang, and J. Rodriguez, "Four consecutive samples based sensorless control for PMSM drives," *IEEE Transactions on Transportation Electrification*, Vol. 10, No. 1, 2082–2094, Mar. 2024.

[3] Garduño, D. M., J. J. R. Rivas, O. C. Castillo, R. O. González, and F. E. R. Gutiérrez, "Current distortion rejection in PMSM drives using an adaptive super-twisting algorithm," *IEEE Transactions on Energy Conversion*, Vol. 37, No. 2, 927–934, Jun. 2022.

[4] Wu, J., J. Zhang, B. Nie, Y. Liu, and X. He, "Adaptive control of PMSM servo system for steering-by-wire system with disturbances observation," *IEEE Transactions on Transportation Electrification*, Vol. 8, No. 2, 2015–2028, Jun. 2022.

[5] Wang, G., D. Wang, H. Lin, J. Wang, and X. Yi, "A DC error suppression adaptive second-order backstepping observer for sensorless control of PMSM," *IEEE Transactions on Power Electronics*, Vol. 39, No. 6, 6664–6676, Jun. 2024.

[6] Chen, L., H. Zhang, H. Wang, K. Shao, G. Wang, and A. Yazdani, "Continuous adaptive fast terminal sliding mode-based speed regulation control of PMSM drive via improved super-twisting observer," *IEEE Transactions on Industrial Electronics*, Vol. 71, No. 5, 5105–5115, May 2024.

[7] Ke, D., F. Wang, X. Yu, S. A. Davari, and R. Kennel, "Predictive error model-based enhanced observer for PMSM deadbeat control systems," *IEEE Transactions on Industrial Electronics*, Vol. 71, No. 3, 2242–2252, Mar. 2024.

[8] Zhang, X., Z. Liu, P. Zhang, and Y. Zhang, "Model predictive current control for PMSM drives based on nonparametric prediction model," *IEEE Transactions on Transportation Electrification*, Vol. 10, No. 1, 711–719, Mar. 2024.

[9] Zhang, J., W. Ren, and X.-M. Sun, "Current-constrained adaptive robust control for uncertain PMSM drive systems: Theory and experimentation," *IEEE Transactions on Transportation Electrification*, Vol. 9, No. 3, 4158–4169, Sep. 2023.

[10] Zhang, X. and Z. Wu, "Two-stage model predictive current control for PMSM drives with parameter robustness improvement," *IEEE Transactions on Energy Conversion*, Vol. 39, No. 2, 1352–1360, Jun. 2024.

[11] Wang, Z., M. Gu, M. Cheng, and W. Hua, "Modeling and predictive control of PMSM considering eddy-current reaction by vector magnetic circuit theory," *IEEE Transactions on Industrial Electronics*, Vol. 71, No. 8, 8491–8502, Aug. 2024.

[12] Zuo, Y., C. Lai, and K. L. V. Iyer, "A review of sliding mode observer based sensorless control methods for PMSM drive," *IEEE Transactions on Power Electronics*, Vol. 38, No. 9, 11 352–11 367, Sep. 2023.

[13] Zhang, Z., X. Liu, J. Yu, and H. Yu, "Time-varying disturbance observer based improved sliding mode single-loop control of PMSM drives with a hybrid reaching law," *IEEE Transactions on Energy Conversion*, Vol. 38, No. 4, 2539–2549, Dec. 2023.

[14] Fliess, M. and C. Join, "Model-free control," *International Journal of Control*, Vol. 86, No. 12, 2228–2252, 2013.

[15] Liu, W., H. Ye, and X. Yang, "Model-free adaptive sliding mode control method for unmanned surface vehicle course control," *Journal of Marine Science and Engineering*, Vol. 11, No. 10, 1904, 2023.

[16] Agoro, S. and I. Husain, "Model-free predictive current and disturbance rejection control of dual three-phase PMSM drives using optimal virtual vector modulation," *IEEE Journal of Emerging and Selected Topics in Power Electronics*, Vol. 11, No. 2, 1432–1443, Apr. 2023.

[17] Guo, X., S. Huang, Y. Peng, K. Lu, S. Huang, D. Luo, and X. Wu, "An improved integral sliding mode control for PMSM drives based on new variable rate reaching law with adaptive reduced-order PI observer," *IEEE Transactions on Transportation Electrification*, Vol. 9, No. 3, 4503–4516, Sep. 2023.

[18] Guo, X., S. Huang, K. Lu, Y. Peng, H. Wang, and J. Yang, "A fast sliding mode speed controller for PMSM based on new compound reaching law with improved sliding mode observer," *IEEE Transactions on Transportation Electrification*, Vol. 9, No. 2, 2955–2968, Jun. 2023.

[19] Song, J., Y.-K. Wang, Y. Niu, H.-K. Lam, S. He, and H. Liu, "Periodic event-triggered terminal sliding mode speed control for networked PMSM system: A GA-optimized extended state observer approach," *IEEE/ASME Transactions on Mechatronics*, Vol. 27, No. 5, 4153–4164, Oct. 2022.

[20] Xu, B., L. Zhang, and W. Ji, "Improved non-singular fast terminal sliding mode control with disturbance observer for PMSM drives," *IEEE Transactions on Transportation Electrification*, Vol. 7, No. 4, 2753–2762, Dec. 2021.

[21] Yang, Y., M. Deng, S. Li, and Y. Zhang, "Based on fast non-singular terminal sliding of PMSM model-free control," *Progress In Electromagnetics Research C*, Vol. 137, 139–153, 2023.

[22] Sun, Z., Y. Deng, J. Wang, T. Yang, Z. Wei, and H. Cao, "Finite control set model-free predictive current control of PMSM with two voltage vectors based on ultralocal model," *IEEE Transactions on Power Electronics*, Vol. 38, No. 1, 776–788, Jan. 2023.

[23] Li, X., J. Liu, K. Zhao, Y. Yin, and L. Zou, "Improved non-singular fast terminal sensor-less sliding mode control of IPMSM considering external disturbance and parameter perturbation," *Progress In Electromagnetics Research B*, Vol. 102, 81–98, 2023.

[24] Chen, L., Z. Jin, K. Shao, H. Wang, G. Wang, H. H.-C. Iu, and T. Fernando, "Sensorless fixed-time sliding mode control of PMSM based on barrier function adaptive super-twisting observer," *IEEE Transactions on Power Electronics*, Vol. 39, No. 3, 3037–3051, Mar. 2024.

[25] Li, X., J. Liu, K. Zhao, Y. Yin, and L. Zou, "An improved model-free sliding mode control algorithm of super-twisting for SPMSM," *Progress In Electromagnetics Research C*, Vol. 135, 195–210, 2023.